Novel production of macrocapsules for self-sealing mortar specimens using stereolithographic 3D printers

Cement and Concrete Composites 142 (2023) 105216

Contents lists available at ScienceDirect

Cement and Concrete Composites

journal homepage: www.elsevier.com/locate/cemconcomp

# Novel production of macrocapsules for self-sealing mortar specimens using stereolithographic 3D printers

Claire Riordan [a,b,*], Giovanni Anglani [c], Barbara Inserra [d], Dave Palmer [b], Abir Al-Tabbaa [a], Jean-Marc Tulliani [d], Paola Antonaci [c]

[a] Department of Engineering, University of Cambridge, Trumpington Road, Cambridge, CB2 1PZ, UK
[b] Micropore Technologies Ltd, Wilton Centre, Redcar, TS10 4RF, UK
[c] Department of Structural, Geotechnical and Building Engineering (DISEG), Politecnico di Torino, Corso Duca Degli Abruzzi 24, 10129, Turin, Italy
[d] Department of Applied Science and Technology (DISAT), Politecnico di Torino, INSTM R.U. Lince Laboratory, Corso Duca Degli Abruzzi 24, 10129, Turin, Italy

ARTICLE INFO

*Keywords:*
Self-healing concrete
Self-sealing
Water absorption
Additive manufacturing
3D printing
Stereolithography
Macrocapsules

ABSTRACT

The use of capsule-based technology for self-sealing and self-healing cementitious systems has been extensively investigated for both macro- and microencapsulated additions. In this study, macrocapsules, produced using a novel technique were characterised and compared, evaluating mechanical triggering, bonding with the cementitious matrix, and self-sealing efficiency upon integration into cementitious mortar specimens. Macrocapsules containing a commercially available water repellent agent were produced in two ways. Stereolithographic additive manufacturing (3D printing) was used to produce novel rigid acrylate macrocapsules as well as alumina ones. Cementitious macrocapsules produced with a rolling technique were also used as a comparison. The capsules were characterised in terms of watertightness, water uptake, and shell morphology. Following this, the capsules were integrated into cement mortar prisms and subjected to controlled cracking by three-point bending to evaluate the triggering and subsequent self-sealing effect. The results highlighted influential process parameters that can be optimised and explored for further capsule-based self-sealing in structural applications.

## 1. Introduction

Self-healing and self-sealing methodologies for improving the durability and longevity of cementitious systems have been increasingly investigated in both academic and industrial settings [1,2]. Microcracking and other structural defects commonly occur within cementitious structures through natural aging, shrinkage, external stresses, and extreme environments. Although this is often managed by routine maintenance, the introduction of self-sealing methodologies can extend the lifespan of a structure through the reduction of water and ionic ingress, thus reducing corrosion, required maintenance, and overall cost [3].

Specifically, macrocapsule-based self-sealing is a mechanically robust and effective methodology, delivering large core volumes to the crack surfaces upon capsule rupture [4,5]. The first use of macrocapsules dates back to the 1990s [6,7]. In the following years, capsule shell materials, such as polymer blends [8], modified cement [9–11], and glass [12–15], have been investigated, aiming to optimise triggering performance within the specimen. Macrocapsule shell and core material largely determine the mechanical characteristics, rupture behaviour, cost, and environmental impact and, thus, the choice can influence their effectiveness and industrial relevance. Often, rigid, brittle shell materials with minimal elongation at rupture are chosen to ensure a triggering response that coincides with the cracking of the cementitious matrix. Araújo et al. investigated this, comparing glass and poly(methyl methacrylate) for consistent rupturing behaviour [12].

The bond between the capsule shell and matrix must also be considered. Rough surfaces are often favoured to avoid capsule slippage prior to complete shell rupture. Anglani et al., for example, used cementitious capsule shells to increase adhesion between the surfaces, as well as to match mechanical characteristics of the capsule and matrix [9,10]. Additional work has investigated the interfacial bond between smoother surfaces through innovative experimental set ups and numerical modelling [16,17]. In order to avoid core material retention, a triggering response with a single break is preferred to that of multiple smaller fractures [4,5].

* Corresponding author. Department of Engineering, University of Cambridge, Trumpington Road, Cambridge, CB2 1PZ, UK.
*E-mail address:* crr41@cam.ac.uk (C. Riordan).

https://doi.org/10.1016/j.cemconcomp.2023.105216
Received 30 April 2023; Received in revised form 5 July 2023; Accepted 19 July 2023
Available online 20 July 2023

The core material must also be considered. Myriad materials have been encapsulated, including adhesives, expansive mineral agents, and other organic binders [10]. The core material and chemical properties, that is, density and viscosity, can affect the release behaviour and the effectiveness of the capsule. These factors, along with larger macrocapsule diameters, facilitate a free-flowing core, thus avoiding a capillary effect that would hinder release [2].

The production method of macrocapsules greatly influences the properties of the shell material and the cost. Prefabricated, cost-efficient glass and polymeric tubes have been used with excellent results. However, the geometry cannot be optimised beyond what is already commercially available. Extrusion and hand-rolling of polymeric and cementitious capsules have also been investigated. These methods, however, created a production bottleneck, reducing their value for large-scale applications. Additive manufacturing (AM), specifically fused deposition modelling (FDM) 3D printing, has also been explored as a method of macrocapsule production. Highly versatile, 3D printing is used in myriad industries, from medical appliances to food to the construction industry, and is increasingly popular because of its cost-effective and time-efficient bespoke manufacturing [8,18–21].

As with other production means, a wide range of materials can be 3D printed, depending on the equipment used. These include metals, ceramics, acrylates, and polymers. Previous work done by Anglani et al. studied how different polymeric filaments used for shell material affected the performance of FDM printed macrocapsules when incorporated into mortar [8]. Although effective, FDM printed parts are often anisotropic, yielding different mechanical characteristics in different areas of the geometry. Watertightness thus decreases, necessitating additional epoxy sealing for core retention.

Stereolithography (SLA), classified as vat polymerisation, is considered superior in accuracy and resolution when compared to FDM printed parts [20,21]. In standard SLA printers, a mobile UV laser is located beneath the resin tray, spot curing a horizontal layer of the photoinitiated resin onto a build platform in a layer-by-layer technique. Because of the positioning of the laser, prints are formed inverted. As each layer is deposited, covalent bonds are formed both in and between the layers, creating a more mechanically homogeneous print. Following printing, the part is “green”, with semi-polymerised resin requiring thermal or UV curing to form additional bonds between the layers. The curing step greatly changes the achieved mechanical and chemical characteristics of the printed parts. A wide range of commercially available resins range in biocompatibility, elasticity, and rigidity post-curing. Because of the wide range of materials available, as well as the accuracy and repeatability achieved, SLA printed parts are often seen in pharmaceutical and health care applications, such as targeted drug delivery [21].

Digital Light Processing (DLP) 3D printing is another inverted printing technique that is gaining in popularity [22]. Similar to SLA, prints can achieve finer levels of detail and accuracy compared to FDM. However, unlike SLA printers, DLP uses a single projected light source to polymerise an entire layer, decreasing the print time. Although DLP printers can be used to print acrylates, in this study ceramic slurry (or ceramic particles suspended in a photoinitiated resin) was used. Because of this material choice, green parts were not cured but rather went through a longer process of resin debinding and sintering. 3D printed ceramics have been studied in detail, investigating the variation in microstructure and mechanical characteristics of printed parts when compared with more traditional ceramic production. Although the material cost and the time required to print are disadvantages, this production method allows geometric flexibility, crucial when designing and optimising new parts. The use of a commercially available ceramic slurry for the fabrication of macrocapsules for self-sealing is a novel combination of shell material and application and, to the best of our knowledge, has yet to be investigated for use in the construction industry.

In this study, another widely used 3D printing technique, SLA, was used to design and produce two different macrocapsules using three different SLA printed materials, comparing their performance with cementitious macrocapsules previously optimised by Anglani et al. [9,10] Acrylate-shell macrocapsules were created using a rigid resin printed on the FormLabs Form3+. Ceramic-shell macrocapsules were formed using an alumina slurry printed on an AdmaTec Admaflex 130. Macrocapsules were closed with a cap printed using an elastic resin on the FormLabs Form2. The design, as well as the printing parameters, were optimised to prioritise watertightness and batch repeatability. The capsules were assessed for triggering behaviour, reproducibility, and self-sealing effectiveness. This work aims to set the stage for more complex and unique geometries of macrocapsules to be printed using SLA. Already, parametric optimisation of the geometry of FDM printed vascular networks and prefabricated macrocapsules has been investigated in De Nardi et al. and Šavija et al., respectively [17,19]. However, as SLA printed macrocapsules have not been studied for self-sealing cementitious applications prior to this, this work aims to understand the mechanical characteristics, triggering behaviour, and sealing effectiveness of these macrocapsules.

## 2. Materials and methods

### 2.1. 3D-printed macrocapsule production: printers and materials

Macrocapsules were printed on three different 3D printers using different materials. FormLabs SLA printers - Form2 and Form3+ (3D Italia, Italy) - were used to print acrylate macrocapsules (FORM) and macrocapsule caps, respectively. Caps were required to seal the macrocapsules and reduce core material leakage. Two commercial photoinitiated acrylate resins, unique to FormLabs printers, were purchased from 3D Italia. The resins were Rigid 10 K (shell material) and Elastic 50 A (cap material) and were used without further purification. Isopropyl alcohol (IPA) was supplied by 3D Italia and used without further purification. Following printing, green parts were washed in IPA for a specified time (material dependent) and thermally and UV-cured for a specified time (material dependent).

A DLP printer ADMATEC Adamflex 130 (ADMATEC Europe, The Netherlands) was used to print ceramic macrocapsules (ADMA). A commercially available photoinitiated alumina slurry (AdmaPrint A130) was purchased from ADMATEC Europe. The slurry is based on a monomer resin system with a photoinitiator (diphenyl(2,4,6,-trimethylbenzoyl)phosphine oxide) and acrylates. Following printing, parts were gently washed using warm water to remove excess slurry. They were then placed in a deionised water bath (37.5 °C) for 24 h to encourage resin debinding. Samples were air-dried for 24 h and oven-dried at 50 °C for 12 h before placing them in a furnace (Carbolite 1200, Carbolite Gero GmbH) for thermal debinding and the sintering step according to the thermal cycle in Fig. 1. The geometry printed was often subjected to delamination and microcracking. Thus, the cleaning, debinding, and sintering procedures were optimised to ensure defect-free macrocapsules. The commercially available characteristics of the different shell and cap materials are presented in Table 1. The optimised printing parameters for FormLabs printers are tabulated in Table 2.

Sikagard-705L, a one-component, solvent-free, low viscosity alkoxysilane water repellent agent (WRA) supplied by Rawlins Paints, was used as a core material for all macrocapsules. Sikagard-705L is commonly used in the construction industry as a waterproofing sealant, hydrophilising surfaces through a process called silanization. Silanization occurs at the cementitious surface as hydroxyl groups replace the alkoxy groups found in the WRA, forming covalent bonds between the silane and the minerals in the cementitious surface.

### 2.2. Macrocapsule design and dimensions

The geometry of the 3D printed macrocapsules was designed on Rhino 7 software (McNeel Europe, Spain). For 3D SLA printed

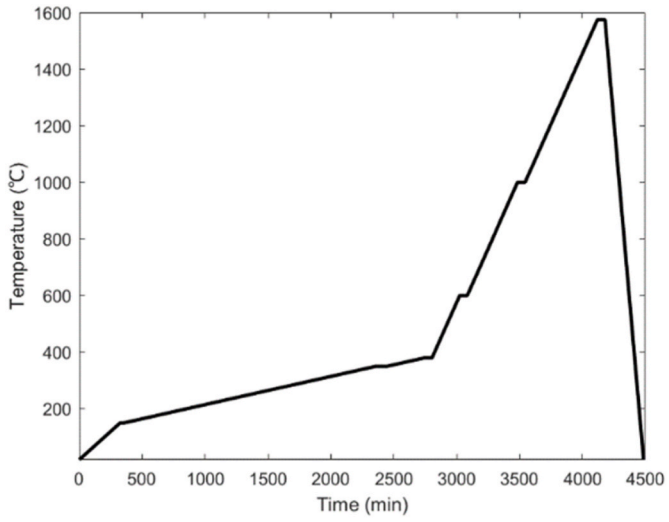


**Fig. 1.** Sintering curve for Ceramic Macrocapsules.

macrocapsules and rolled cementitious macrocapsules (CEM), whose production method and triggering response were already established (see Anglani et al.) [10], a cylindrical capsule was used with a cap (Fig. 2). Printed capsule lengths for FORM and ADMA capsules can be found in Table 3. There was some dimensional variation between FORM and ADMA macrocapsules because of printer limitations and additional shrinkage in the z-direction during sintering. To ease assembly and allow for any variation in batches, flexible acrylate (Elastic 50 A) was favoured for the cap, sliding over the top of the capsule and covering 5 mm of the body. The design prioritised printing simplicity, facilitated ease of assembly, and watertightness, thus requiring minimal epoxy ensured watertightness.

Batch reproducibility was assessed for both the Form3+ and the Admaflex 130, by measuring the standard deviations of the capsule thickness and height (Table 3). Although the capsules showed no major visual defects, some variation between batches was seen. This might have been caused by the vertical printing position of the capsule with respect to the build plate and any possible blowout that occurred from this orientation. Printing the capsules at an angle or horizontally may reduce blowout but will increase the capsule strength when triggering because of the orientation of the layers. Additionally, any excess slurry remaining after cleaning may alter the final measurements.

### 2.3. Shell material testing

Previous results from Anglani et al. have highlighted the importance of creating a watertight macrocapsule for core retention [8]. For cementitious capsules, this is achieved with bulbous epoxy caps with an internal epoxy coating. In this study, printed caps (Fig. 2) minimised the amount of epoxy coating required. Watertightness (WT) was measured accurately to four decimal points, according to the following procedure. Capsules were filled with a known volume of water, sealed with a cap, and a thin layer of epoxy was applied at the junction between shell and cap, and stored in laboratory conditions (20 °C). The mass change was measured at 1-h increments for a period of 24 h with one additional reading at 48 h by means of an analytic balance (Sartorius, Germany, 0.1 mg accuracy). Equation 1 calculates the percentage of remaining water after "x" hours.

$$WT = \frac{Mx}{Mi} * 100$$

$$Mx = mass\ after\ ''x''\ hours$$

$$Mi = intial\ mass$$

Equation 1. Equation of percentage mass loss as a measure of watertightness.

Water uptake (WU) of the shell material was also measured. Shell material was fully immersed in water and stored in laboratory conditions (20 °C) and weighed at 24 h and 48 h. Equation 2 calculates the percentage of absorbed water after "x" hours.

$$WU = \frac{Mx - Mi}{Mi} * 100$$

$$Mx = mass\ after\ ''x''\ hours$$

$$Mi = intial\ mass$$

Equation 2. Equation of percentage of mass gain as a measure of water uptake.

### 2.4. Mortar specimen preparation

Unreinforced mortar prisms (40 mm × 40 mm x 160 mm) were made using Ordinary Portland Cement (CEM I 42.5 R) (Buzzi Unicem, Italy), tap water (with a water to cement ratio of 0.5), and 0–2 mm normalised sand (with a sand to cement ratio of 3) (Matest, Italy). The mortar was prepared according to standard EN 196–1. Macrocapsules were pre-placed in the moulds before filling with mortar (Fig. 3). To do so, nylon string was tightly stretched across the mould. The exact placement is illustrated in Fig. 4. A U-shaped rod was placed in the mould to create a U-shaped notch, 4 mm in width and 5 mm in height, to aid cracking of the specimen. The capsules were placed centrally and equidistant from the sides onto the thread and held in place with an acrylate glue. This method for capsule placement followed previous work done by Anglani et al. [10] Furthermore, the correct positioning of the capsules with respect to the bottom the specimen was verified in all cases when the specimens were split open after testing (as in Fig. 18b). For each specimen, two macrocapsules were placed in the mould, both containing WRA. Specimens were covered with plastic sheets and placed in a humid environment (60% relative humidity) with a constant temperature of 20 °C ( ± 2 °C). After 24 h, specimens were demoulded and recovered with plastic sheets and placed back into the previous environment (60% relative humidity, 20 °C [± 2 °C]).

**Table 2**
Printing parameters of the FormLabs printer.

| Parameter | Form2 | Form3+ |
|---|---|---|
| Layer height (mm) | 0.1 | 0.1 |
| XY Resolution (mm) | 0.025 | 0.025 |
| UV Wavelength (nm) | 405 | 405 |
| Layer Spot Size (mm) | 0.140 | 0.085 |
| Curing Temperature (°C) | 60 | 70 |
| Curing Time (min) | 20 | 60 |

**Table 1**
Commercially available mechanical characteristics of 3D printed materials.

| Material | Printer | Tensile strength (MPa) | Flexural strength (MPa) | Flexural modulus (GPa) | Elongation at rupture (%) | Shore Hardness |
|---|---|---|---|---|---|---|
| Elastic 50 A | Form2 | 3.23 | – | – | 160 | 50 A |
| Rigid 10 K | Form3+ | 65 | 126 | 9 | 1 | – |
| Admaprint 130 | Admaflex 130 | – | 415 | 360 | – | – |

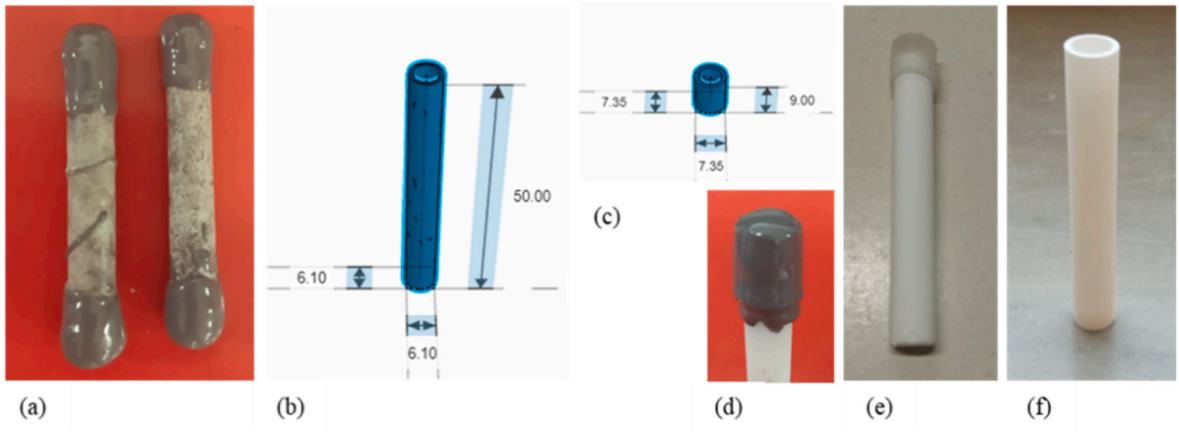


**Fig. 2.** (a) Rolled cementitious macrocapsules with epoxy-coated ends (b) Cylindrical design for 3D printed macrocapsules (c) 3D printed cap design for operational ease and minimal water loss (d) 3D printed acrylate macrocapsule with elastic cap with epoxy resin (e) 3D printed acrylate macrocapsule with elastic cap prior to fixing with epoxy resin (f) 3D printed ceramic capsule (without cap) post-sintering step.

**Table 3**
Investigation of batch reproducibility and capsule variability.

| | FORM | ADMA |
|---|---|---|
| | Average (mm)/Std. dev. | Average (mm)/Std. dev. |
| **Shell thickness** | 0.68/0.02 | 0.85/0.03 |
| **Shrinkage (% in x & y direction)** | – | 20.2 |
| **Length** | 50.53/0.41 | 45.51/0.53 |
| **Shrinkage (% in z direction)** | – | 24.6 |

### 2.5. Specimen cracking and macrocapsule triggering

At day seven, the specimens were cracked via a crack-mouth opening displacement (CMOD) controlled three-point bending test (Fig. 5) with a span of 10 cm using a 250 kN closed-loop MTS hydraulic press (MTS, USA). The target maximum residual crack width was set at 300 μm with the unloading point based on trial specimens not included in this paper. However, variation in the residual crack width did occur because of the different mechanical properties of the macrocapsules. If capsule rupture did not occur, the specimen continued to be loaded until rupture did occur. After cracking, specimens were stored in a dry laboratory environment, crack face downwards, for at least 24 h to allow release of the core material.

During the cracking process, core release could be clearly seen on the sides of the specimens (Fig. 5). The width of the crack mouths was measured using stereoscopic images. Three defect-free locations along the crack path were marked with five measurements taken at each location. The average crack width for the specimen was calculated as an average of the 15 measurements. Variation was seen in the cracks because of variations in macrocapsule material and consequent triggering.

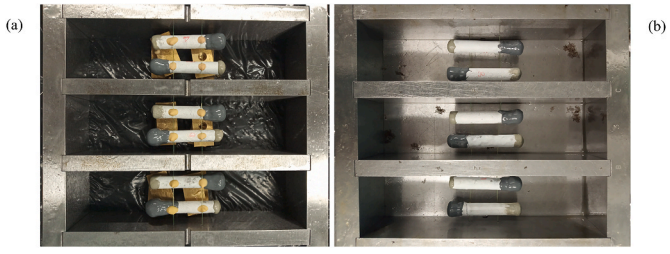


**Fig. 3.** (a) Placement of macrocapsules in moulds – bottom view (b) Placement of macrocapsules in moulds – top view.

### 2.6. Capillary water absorption

The water absorption through capillary action in a cementitious matrix is greatly determined by the porous nature of the matrix, the inclusion of cracks in the matrix, as well as the respective widths and tortuosity of the cracks. As capsules are mechanically triggered and core

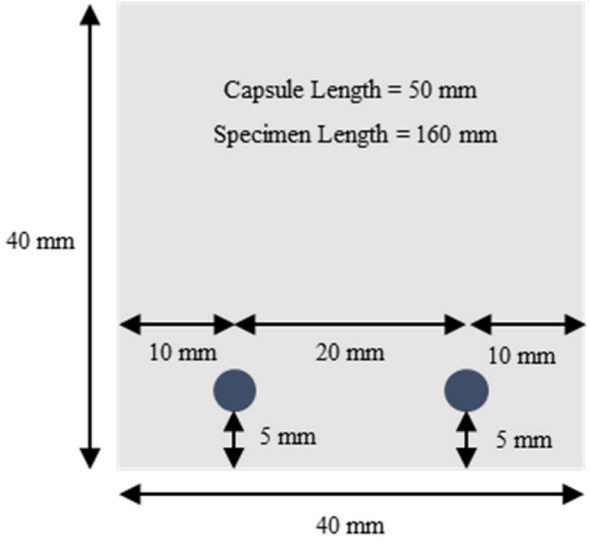


**Fig. 4.** Cross section of mortar specimen containing two macrocapsules (all dimensions in mm).

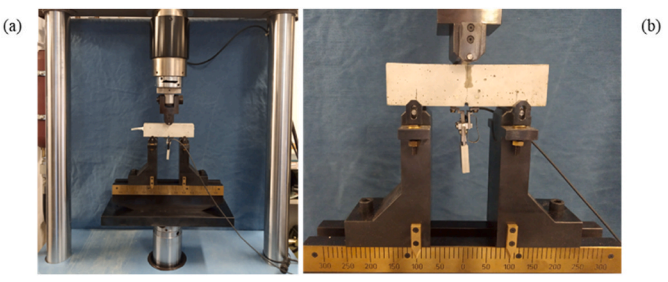


**Fig. 5.** (a) Three-point bending test set up with a specimen in place (b) Core release seen on the side of the specimen.

material (WRA) is released onto the crack surface, the self-sealing response is initiated, specifically silanization (see section 3.1). The silanization reaction hydrophobises a surface and reduces water absorption, thus correlating sorptivity (water absorption rate) and self-sealing effectiveness.

The capillary water absorption test was conducted in agreement with Van Mullem et al. [15] Namely, specimens were placed in a 40 °C oven for 14 days prior to testing water absorption to ensure a constant weight, that is, less than a 1% weight decrease in a 24-h period. Following this, specimens were then kept in a 20 °C laboratory environment for an additional day. To ensure that water absorption occurred only at the crack opening, the sides of specimens, including the sides of the crack and the bottom of the specimen (except the notch area), were waterproofed using aluminium tape. Slight adjustments were made if there were deviations or irregularities in the crack path. The specimens were then weighed.

The set up is illustrated in Fig. 6. Specimens were placed onto spacers to ensure the crack surface was completely in contact with water. The water level was maintained at 8 mm (± 1 mm) from the bottom of the specimen. At selected time intervals over a 24-h period (after 10 min, 20 min, 30 min, 1 h, 1 h 30 min, 2 h, 3 h, 4 h, 6 h, 8 h, and 24 h), one specimen was removed from the water, ensuring no water splashed into the crack, and carefully blotted with a damp cloth to remove excess water. The specimen was then weighed and placed back onto the spacers. This was repeated for all specimens. They were weighed in the same order for specified time intervals until 24 h. Reference samples (cracked but not containing macrocapsules) and uncracked samples were waterproofed in the same method to ensure comparable multi-directional flow throughout the mortar surface.

The results were plotted with the square root of time on the x-axis (h) and the water uptake (g) on the y axis. The slope of the line was taken as the sorptivity coefficient (SC). The sealing efficiency of the specimen was calculated using the equation below.

$$SE = \frac{SC_{REF} - SC_{CAP}}{SC_{REF} - SC_{UNCR}}$$

$SE = sealing\ efficiency$

$SC_{REF} = sorptivity\ coefficient\ of\ reference\ specimen$

$SC_{CAP} = sorptivity\ coefficient\ of\ capsule - containing\ specimen$

$SC_{REF} = sorptivity\ coefficient\ of\ uncracked\ specimen$

Equation 3. Equation for calculating percentage sealing efficiency based on the water absorption of a self-sealed mortar matrix.

### 2.7. Mechanical characteristics of printed material

#### 2.7.1. Tensile strength test

Macrocapsules of different shell materials were assessed in a tensile strength test inspired by Hilloulin et al. [25] For the ADMA and FORM series, tubes were printed with the same dimensions as the macrocapsules. For the CEM series, tubes were hand-rolled into the same dimensions as the macrocapsules. For all materials, clay-like epoxy was applied onto the ends of the tubes, creating a bulb that extended down the length of the tube by 1 cm on either end. A stainless steel hook was pressed into the epoxy and the epoxy was smoothed around it. Tubes were left to harden for one week. Once hardened, the tube was attached via the hooks to a 1 kN electromechanical press (MTS, USA, Fig. 7). This facilitated a hinge-like motion, allowing rotation at the extremities and optimal positioning of the tube along the axial loading direction. The test was run at an elongation rate of 5 mm/min until the capsules broke or there was failure of the surrounding epoxy.

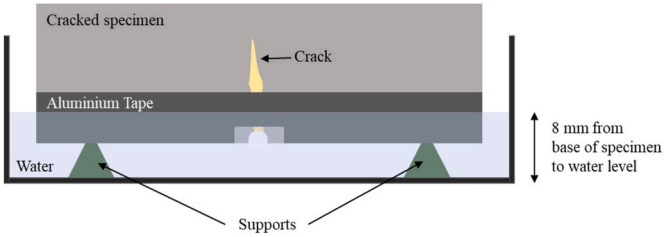


**Fig. 6.** Set up of capillary water absorption test.

#### 2.7.2. Flexural strength test

As in section 2.7.1., for the ADMA and FORM series, tubes were printed with the same dimensions as the macrocapsules and, for the CEM series, tubes were hand-rolled into the same dimensions as the macrocapsules. Tubes were then laid onto the semicircular supports of a 1 kN electromechanical press (MTS, USA, Fig. 8). Clay was used to aid the positioning of the tube prior to the test, ensuring that there was no movement or slippage when the force was applied. The span between the supports was 25 mm. The test was run with a deflection velocity of 5 mm/min until the capsules cracked to failure.

#### 2.7.3. Bond strength test

Macrocapsules of both shell materials were assessed in a bond strength test. Like the tensile test described in section 2.7.1, the test set up was inspired by Hilloulin et al. [25] Epoxy was applied onto the open end of the microcapsule, creating a bulb that extended down the length of the tube by 1 cm. A stainless steel hook was pressed into the epoxy and the epoxy was smoothed around it. They were left to harden for one week. Unreinforced mortar prisms (40 mm × 90 mm x 160 mm) were made using the same mix design and curing conditions as reported in section 2.4. A macrocapsule was pre-placed vertically in the mould before filling with mortar. The capsule was placed centrally and equidistant from the sides with 25 mm of its length embedded in the specimen. Once cured, the specimens were bolted onto the base of the same 1 kN electromechanical press as for the tensile and flexural tests described in section 2.7.1 and 2.7.2. The hook at the top of the macrocapsules was attached to the testing machine using a clip (Fig. 9). The test velocity was set to 5 mm/min and the test was run until there was slippage of the macrocapsule from the matrix or breakage of the macrocapsule, whichever occurred first.

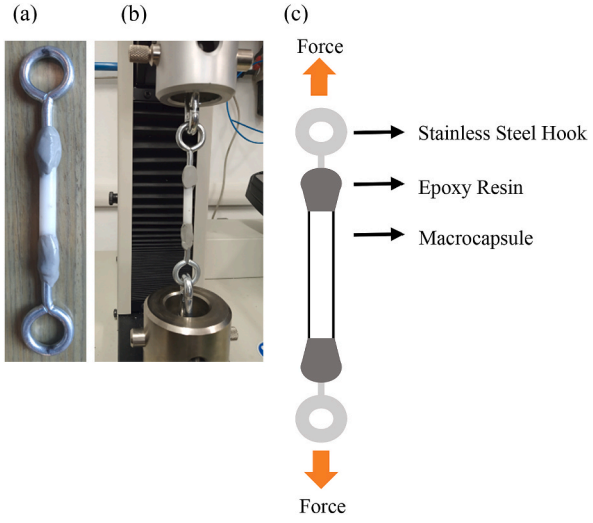


**Fig. 7.** (a) Macrocapsule with epoxied hooks on both ends (b) Tensile strength set up (c) Diagram further explaining tensile strength set up.

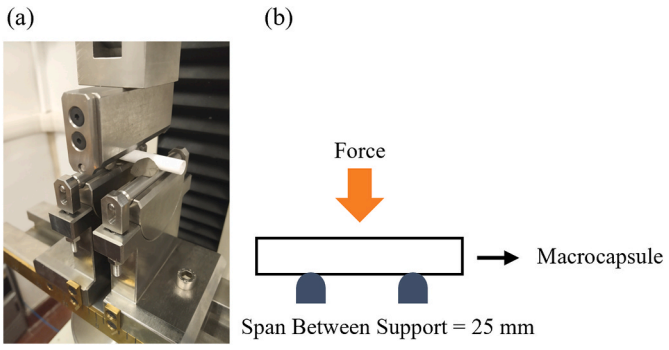


**Fig. 8.** (a) Flexural strength set up (b) Diagram further explaining flexural strength set up.

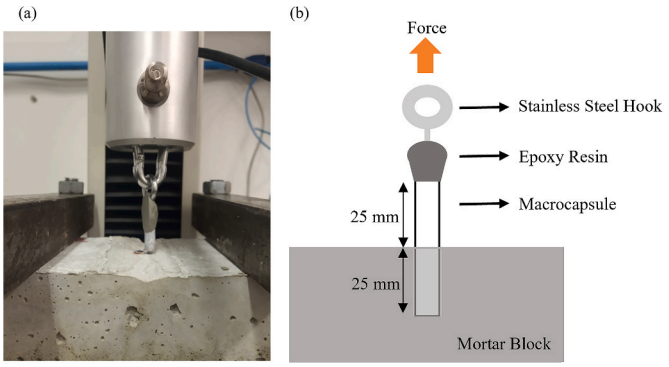


**Fig. 9.** (a) Bond strength set up (b) Further explanation of bond strength set up.

### 2.8. SEM

Shell material was imaged using scanning electron microscopy (FEI Corp., Nova NanoSEM 450, USA) under 8 kV accelerating voltage to better visualise the printed layers and thus understand the rupture behaviour and mechanical characteristics. Shell materials were kept at room temperature and mounted on aluminium stubs. Prior to SEM imaging, samples were gold sputtered.

## 3. Results and discussion

### 3.1. Shell material characterisation

Table 4 reports the changes in capsule mass over time, measuring watertightness. For all shell materials, there was less than 0.1% mass lost over a 24-h period, validating the security of the cap sealed in epoxy. Although using a scale accurate to four decimal points, the variation reported below may result from filling error instead of material differences. For the FORM and ADMA capsules, no additional epoxy was required on the interior or exterior of the capsules to achieve minimal mass lost. However, as previous work demonstrated the necessity for internal epoxy on cementitious capsules, this coating was applied for the CEM series.

The weight increase of the shell material after being fully submerged in water for 48 h is tabulated below (Table 5). Measurements were taken at both 24 h and 48 h but remained stable for the intermittent 24 h, so only the final measurement is reported. Rigid acrylate-based materials show minimal water uptake, with 0.6% mass increase. With this minimal amount of water ingress, core stability was preserved. Additional epoxy coating may reduce water ingress further but must be weighed against the increased preparation time that it would require. The choice is core dependent. For cementitious capsules, epoxy is required to achieve the low increase in mass as presented here. The cap material increased the greatest amount and thus the choice to epoxy coat the cap was validated.

**Table 4**
Watertightness of macrocapsules characterised by percentage decrease in mass.

| Shell Material | Percentage decrease in mass (%) |
|---|---|
| Rigid 10 K | 0.06 |
| Ceramic | 0.05 |
| Cementitious | 0.09 |

### 3.2. Crack creation and variation in measured crack width

Figs. 10 and 11 show the average residual crack width (μm) obtained for each of series: ADMA, CEM, FORM, and REF.

The narrowest average crack width (270 μm) was seen in the CEM series, while the largest (465 μm) was seen in the FORM series, which also showed the greatest standard deviation. This behaviour can be explained by the addition of rigid macrocapsules within the specimen, as well as the characteristics of the shell. Macrocapsules hindered crack width reproducibility and increased the range of crack widths obtained as the macrocapsules acted as physical barriers to elastic crack closure. Fig. 11 highlights the variation in residual crack widths for each specimen series while Fig. 12 illustrates the load vs. displacement graphs of each series. The ADMA series had minimal variation amongst its residual crack widths. However, despite unloading at the same measured crack with, the residual crack widths of the ADMA series were, on average, greater than that of the CEM or REF series, possibly because of capsules hindering elastic crack closure. The ADMA macrocapsules greatly increased the strength of the specimens at early-stage loading. However, the brittle nature of the ceramic shell was also apparent. Fig. 12 depicts the large, sharp load drops, signaling an ADMA capsule rupture. Additionally, the capsules' triggering behaviour was repeatable, demonstrating the benefit of DLP additive manufacturing and the capsules' layer-by-layer formation.

For the CEM series, the residual crack widths were comparable to that of the reference series. This can be explained by the compatible cementitious shell material of the macrocapsule, which exhibited similar mechanical and chemical characteristics to the main matrix. Unlike the sharp load drops seen in the ADMA series, CEM macrocapsules showed less pronounced load drops, possibly indicating a convoluted or bifurcated crack path through the shell of the macrocapsule. This can be largely explained by its manufacturing process – hand rolling – which led to variation in shell thickness and contrasts with the more exact additive manufacturing techniques used for ADMA and FORM capsule fabrication.

The FORM series displayed the greatest amount of variation amongst the different series for both residual crack width and triggering behaviour. There was a distinct lack of repeatable triggering behaviour. It was hypothesised that this was because there was partial filling of the grooves between layers with excess resin during the capsule fabrication, creating a too-strong-for purpose capsule that acted as a pseudo-rebar. This is illustrated in Fig. 12 as there is strain hardening behaviour until complete capsule rupture, after which there is immediate elastic crack closure. Furthermore, small load drops followed by continued strain hardening behaviour were seen prior to capsule rupture. This may

**Table 5**
Water uptake of shell material characterised by percentage increase in mass.

| Shell Material | Percentage increase in mass (%) |
|---|---|
| Rigid 10 K | 0.6 |
| Elastic 50 A | 4 |
| Ceramic | 0.8 |
| Cementitious with Epoxy | 0.9 |

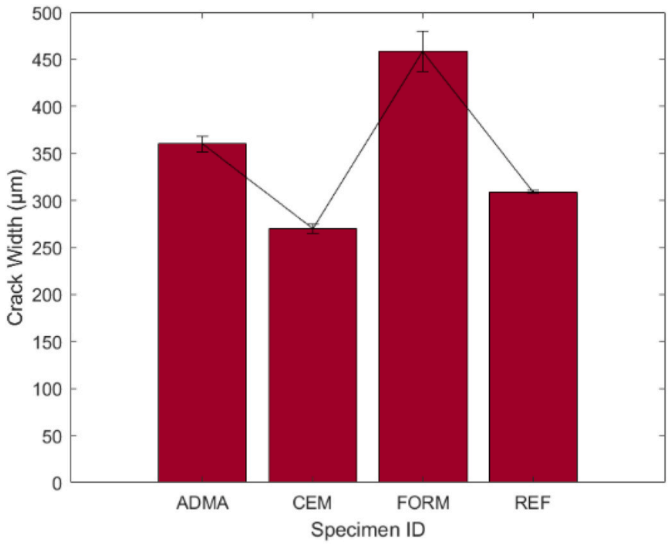


**Fig. 10.** Variations in crack widths of specimens.

indicate partial fracturing or decentralised splintering of the capsules, causing variation in the core release. Finally, it was hypothesised that the mechanical characteristics of the shell material may not be homogeneous. The resin used is composed of two photoinitiated acrylates and has a large percentage of unspecified filler (55–75% according to the commercially available safety data sheet). Although the printer automates the stirring of the resin in the resin bath prior to the printing of each layer, the homogeneous distribution of the filler is difficult to validate. Further mechanical testing of the macrocapsule was required following specimen cracking and will be discussed in section 4.5 onwards.

Given the large capsule diameter necessary to overcome resistive capillary forces, and the large quantity of core material, a visual core release was expected following triggering of the macrocapsules. In the ADMA and CEM series, this was seen (Fig. 13). However, in the FORM series, it was not.

Core release was seen in FORM specimens in the hours following cracking, indicating a slow seepage from the triggered capsules. It is thought that capillary forces were not restricting flow out of the capsule, given the identical core volume and similar geometries. This difference in behaviour may be beneficial, with some literature noting that slow triggering could potentially increase the surface area covered by the core

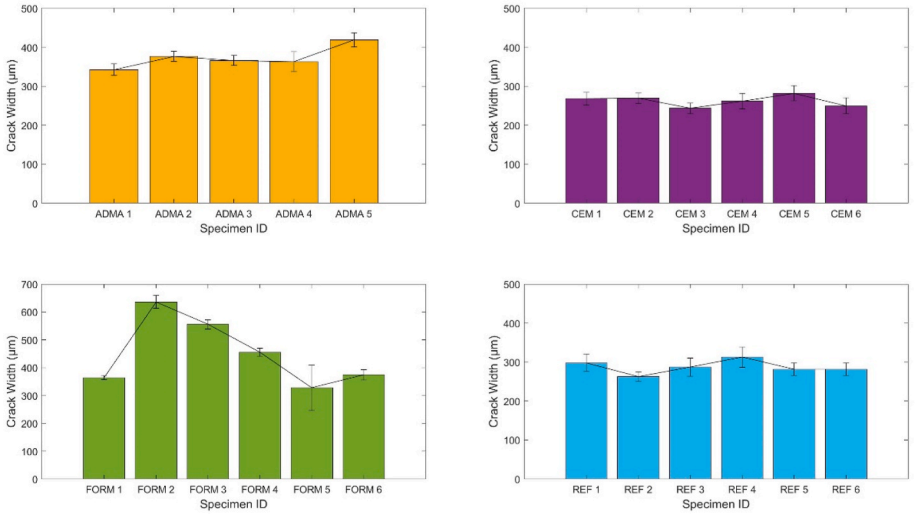


**Fig. 11.** Variation in crack width of specimens comparing each series.

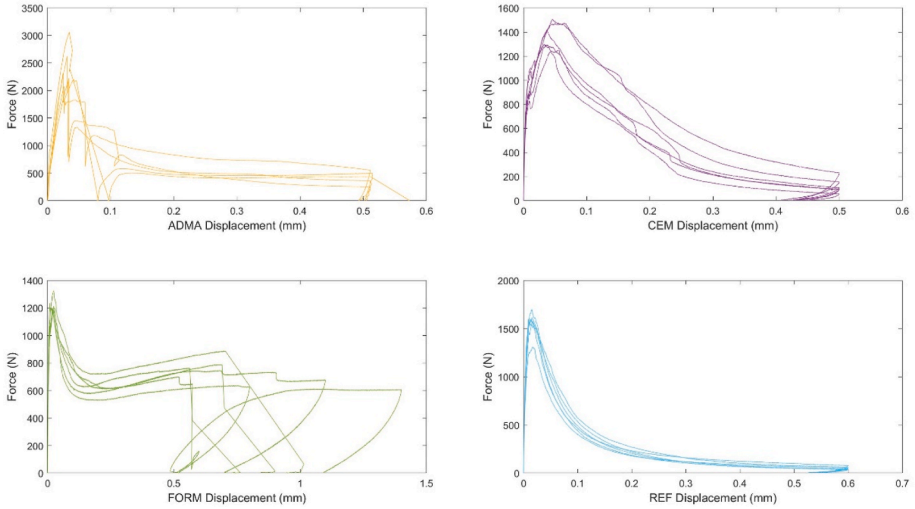


**Fig. 12.** Variation in macrocapsule triggering behaviour for the different specimen series, as highlighted through the related Force vs. Displacement curves.

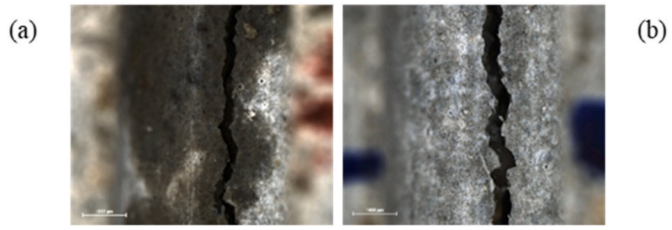


**Fig. 13.** (a) Visual core release seen in an ADMA specimen (darker areas denoting WRA absorption into the mortar matrix) (b) Lack of core release in a FORM specimen.

[23,24].

### 3.3. Capillary water absorption of mortar specimens

Figs. 14 and 15 depict the water absorption of the different specimen series over time. The ADMA and CEM series show excellent waterproofing with minimal variation, matching, or in the case of the CEM series, outperforming the uncracked specimens (Table 6). As there was capsule triggering and visual confirmation of core release, this was a predicted result. Future work might look at quantifying the core volume and capsule dosage required to maintain the self-sealing effect. The FORM series performed only slightly better than that of the REF series and with a large amount of variation. Although there was visual confirmation of core release, albeit hours after cracking, it is hypothesised that the volume released was too small to ensure adequate surface covering and waterproofing.

### 3.4. Mechanical characteristics of shell material

The tensile behaviour of the macrocapsules is depicted in Fig. 16. When uniaxial tensile force was applied, brittle behaviour was observed for all macrocapsule shell materials. This contrasts with the partial fracturing seen in Fig. 12 for the FORM and CEM series capsules. This change in behaviour can be partially attributed to the type of test, which does not correctly represent the forces felt by the macrocapsules when they are embedded in the cementitious matrix. Despite all capsules exhibiting brittle breakages, there were differences between the series' behaviour. The FORM series capsules elongated further, with 1.27% strain at rupture, and required greater force on average (326 N) than ADMA capsules (151 N) and CEM capsules (180 N). Despite the high tensile strength of alumina ceramics, the horizontal layer-by-layer formation of the ADMA macrocapsules explains why less force was required for rupture. However, interestingly, the FORM series exhibited the greatest tensile strength, despite its layer-by-layer formation. This unexpected behaviour harkens back to the inconsistent triggering of the FORM series depicted in Fig. 12 and further supports the hypothesis that the grooves between the layers are partially filled with excess resin during the curing process, leading to a stronger material.

The flexural strength of the macrocapsules further illuminated the different triggering behaviour of the shell materials (Fig. 17). The ADMA and CEM series fractured centrally, with ADMA capsules breaking at the junctions between their printed layers. ADMA capsules required the greatest force (647 N) but underwent the least change in displacement, consistent with their high stiffness and brittle mechanical properties. CEM capsules were significantly weaker, requiring only 145 N to successfully trigger, but showed consistent and relatively sharp breaks. FORM capsules, on the other hand, exhibited smaller load drops before failure. This was seen to correlate with decentralised splintering or partial fracturing of the shell and is consistent with capsule triggering behaviour seen in Fig. 12 and the hypothesis of heterogeneous capsule shells. Additionally, this flexural behaviour helps to explain the lack of visual confirmation of core release from FORM series macrocapsules and, consequently, the poor self-sealing. If capsule rupture is decentralised or only partial, the release of the core material may not align with the crack mouth. Although work has been done using ridges to guide macrocapsule breakage [19], for the FORM series the use of ridges or guides may not be successful as capsule triggering is not repeatable.

The bond strength test (section 2.7.3) aimed to measure the bond strength between the macrocapsule shell and the cementitious matrix. However, rupture of the capsule occurred before slippage so an accurate bond strength could not be measured. Instead, the maximum force (Fig. 18) or stress, 0.77 MPa and 0.27 MPa for FORM and ADMA capsules respectively, required for capsule failure embedded in a cementitious matrix was measured. Compared to non-embedded capsules placed into tension (Fig. 16), solely brittle behaviour was not seen. FORM series capsules underwent partial fracturing as denoted by the small load drops. This result agrees with previous mechanical testing and aids the conclusion that the FORM capsules are not suited for repeatable, localised fracture. On the other hand, ADMA series capsules exhibited some plastic behaviour. This could potentially be due to some delamination of layers prior to complete rupture. For both capsules, this test increased confidence in the lack of capsule slippage during the specimen cracking and capsule triggering. To further illustrate this, a cracked specimen

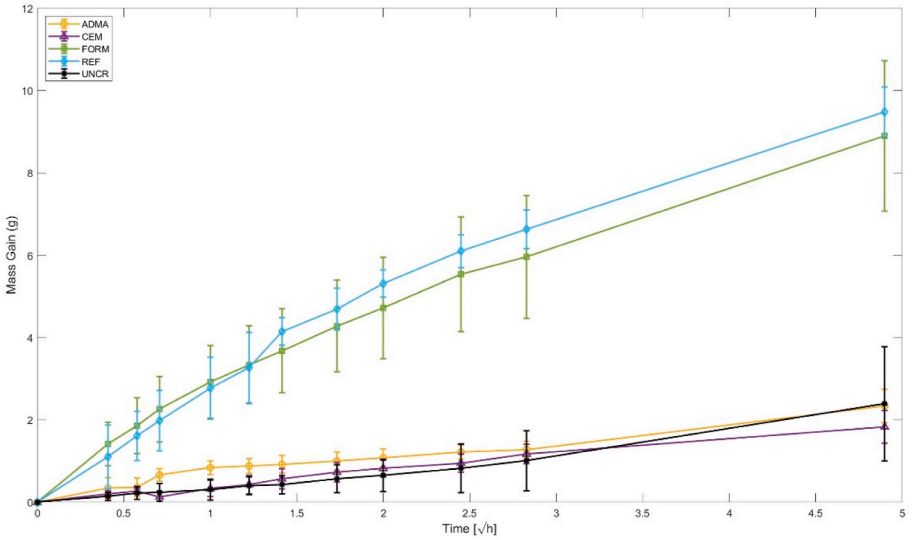


**Fig. 14.** Water absorption of the specimens over time.

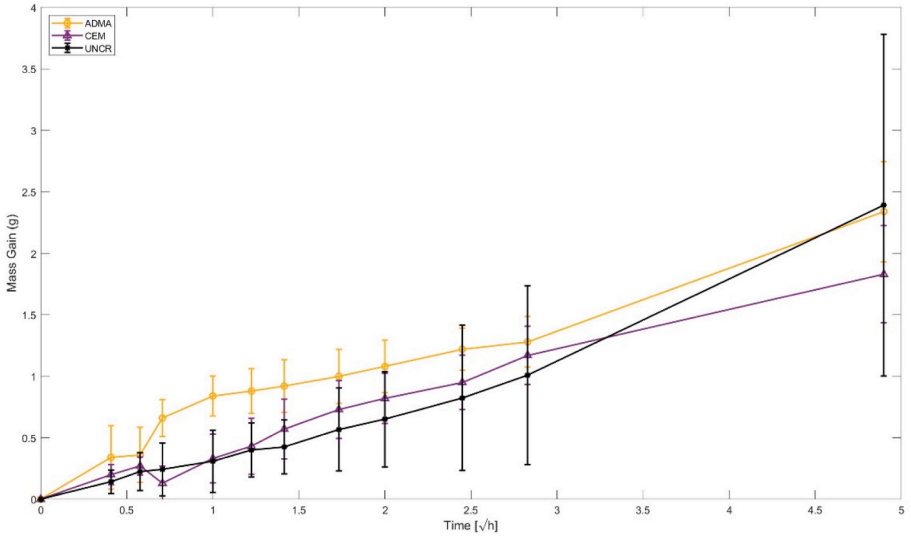


**Fig. 15.** Water absorption of ADMA, CEM, and UNCR series over time.

**Table 6**
Sealing efficiency of the specimen series.

| Series Names | Sorption coefficient, $S$ (kg/(m$^2$·h$^{0.5}$)) | Sealing efficiency, $SE$ (%) |
|---|---|---|
| REF | 1.89 | – |
| UNCR | 0.48 | – |
| ADMA | 0.51 | 98 |
| CEM | 0.41 | 105 |
| FORM | 1.65 | 17 |

containing FORM macrocapsules was fully opened to show the two capsules still embedded in the matrix (Fig. 18).

Macrocapsule shell material and cap material were imaged by SEM to visualise the printed layers formed during the additive manufacturing processes. FORM macrocapsules are seen in Fig. 19, with less distinct layers compared to the ADMA and the caps. FORM capsules take on a more homogeneous appearance when compared to other 3D printed parts, which can be beneficial in principle but for this application was detrimental to triggering. This could be in part due to the viscous resin and filler depositing in the grooves between the layers. ADMA capsules, in contrast, exhibited a clear layered structure, evident in the triggering behaviour that was seen.

## 4. Conclusions

This work investigated the design and production of SLA and DLP 3D printed macrocapsules for use in self-sealing mortar specimens. Two different macrocapsules, with acrylate shell (FORM) and ceramic shell (ADMA), were assessed in comparison to traditional cementitious macrocapsules for their triggering behaviour and self-sealing response, with additional mechanical testing to further characterise the capsule shell material and better understand variations in rupture behaviour. FORM macrocapsules were composed of a rigid 10 K shell printed on a Form3+ printer. ADMA macrocapsules were composed of an Admaprint 130 alumina shell printed on an Admaflex 130. Both were closed using Elastic 50 A caps printed on a Form2, followed by a thin layer of epoxy resin at the junction between shell and cap material. The main conclusions are summarised below.

1. During three-point bending tests, the lack of repeatable ruptures and the convoluted fracturing patterns of FORM macrocapsules confirmed that FORM capsules were not triggering effectively at the

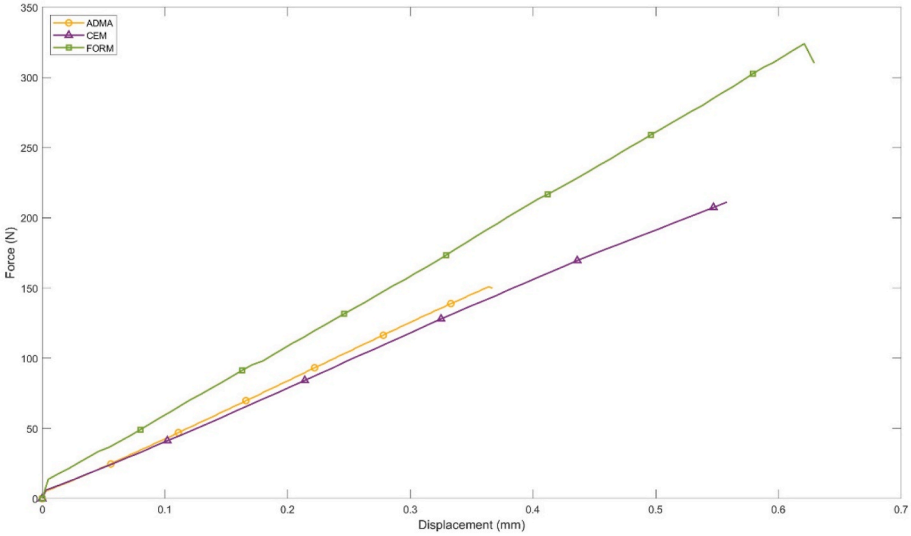


**Fig. 16.** Tensile behaviour of the macrocapsules.

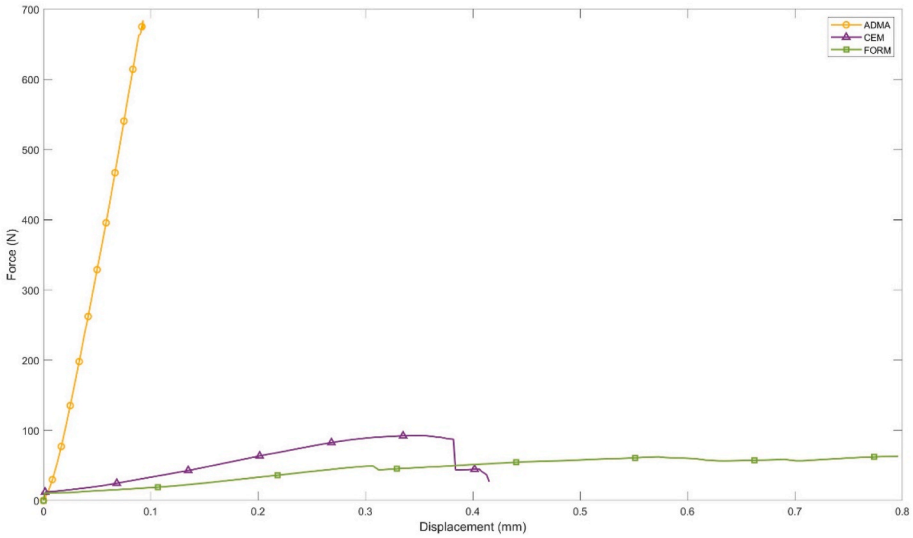


**Fig. 17.** Flexural behaviour of the macrocapsules.

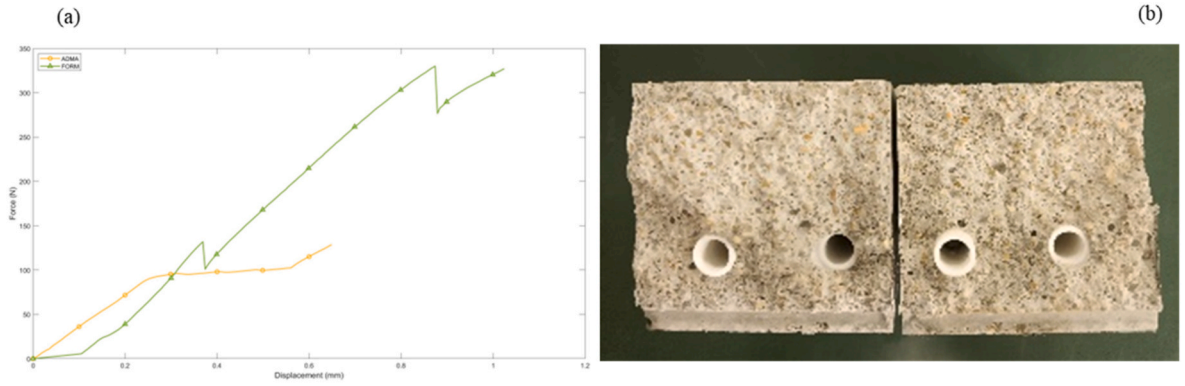


**Fig. 18.** (a) Results of the pull-out tests performed on the 3D printed macrocapsules (b) Opened specimen containing FORM macrocapsules.

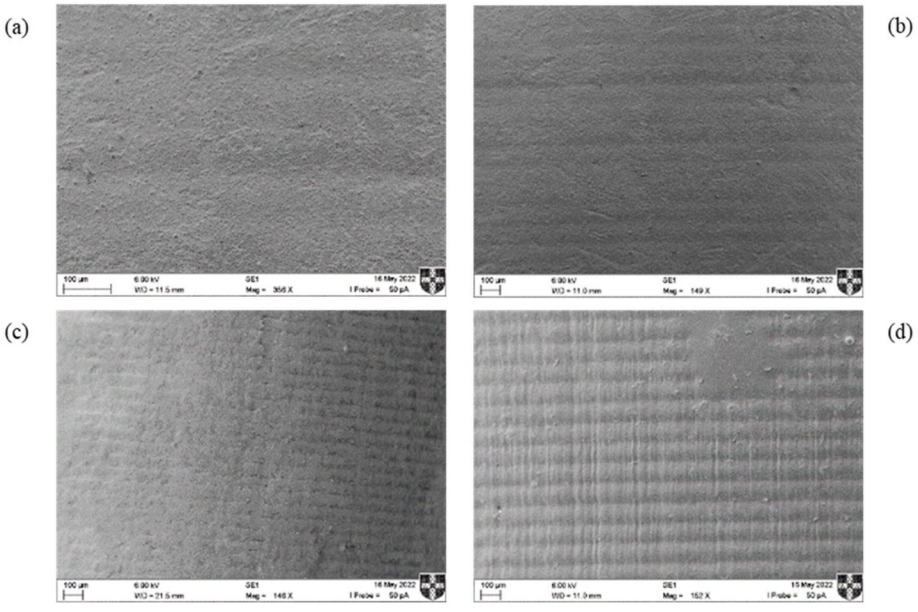


**Fig. 19.** SEM images of (a & b) FORM shell material (c) ADMA shell material (d) cap material.

additive layer junctions as expected, given the manufacturing process used.
2. The SEM images of FORM macrocapsules, compared to ADMA macrocapsules, further illustrated the above point. FORM layers were not as clear, with some of the grooves seemingly filled in with additional material.
3. Because of the unique rupturing patterns seen with FORM macrocapsules, it was not verified that there was complete core release at the crack mouth of the mortar specimen. This was validated by the poor sealing efficiency, quantified using a water absorption test. There may have been an overall waterproofing effect, however, that was not quantified in this work.
4. In contrast, ADMA macrocapsules ruptured in a repeatable manner during three-point bending. The repeatability was comparable to that of the cementitious macrocapsules.
5. ADMA macrocapsules effectively sealed the crack mouth of the mortar specimens, demonstrating 98% sealing efficiency. This was comparable to the sealing efficiency of the cementitious capsules (105%).
6. In addition to varying the rupture pattern, the shell materials greatly affected the load required before rupture in the three-point bending test and thus the achieved crack width. This may also have contributed to the variation seen with the self-sealing behaviour.
7. For both 3D printed capsules, the bond strength between the capsule shell and the matrix was satisfactory, with no slippage detected. This was measured using a half-embedded macrocapsule that was placed under pull-out loading conditions until tensile failure or slippage. Additional visual inspection confirmed that capsules were not slipping during specimen cracking.
8. Although FORM capsules used less costly material and were faster to fabricate, they did not seal the mortar specimen to the same extent as ADMA and CEM. In future work, FormLabs acrylate material could be used to preliminary study the effects of different capsule geometries on the overall mechanical behaviour, before transferring these geometries to ceramic or cementitious shell material.

## Declaration of competing interest

The authors declare that they have no known competing financial interests or personal relationships that could have appeared to influence the work reported in this paper.

## Data availability

Data will be made available on request.

## Acknowledgments

This project has received funding from the European Union's Horizon 2020 research and innovation programme under the Marie Skłodowska-Curie grant agreement No 860006.

## References

[1] K. van Breugel, Is there a market for self-healing cement-based materials?, in: 1st International Conference on Self-Healing Materials, 2007.
[2] K. Van Tittelboom, N. De Belie, Self-healing in cementitious materials-a review, Materials 6 (6) (2013), https://doi.org/10.3390/ma6062182.
[3] M. De Rooij, E. Schlangen, C. Joseph, Self-Healing Phenomena in Cement-Based Materials, vol. 1, Springer, 2013.
[4] V.C. Li, Y.M. Lim, Y.W. Chan, Feasibility study of a passive smart self-healing cementitious composite, Compos. B Eng. 29 (6) (1998), https://doi.org/10.1016/S1359-8368(98)00034-1.
[5] C. Joseph, A.D. Jefferson, B. Isaacs, R. Lark, D. Gardner, Experimental investigation of adhesive-based self-healing of cementitious materials, Mag. Concr. Res. 62 (11) (2010), https://doi.org/10.1680/macr.2010.62.11.831.
[6] C. Dry, Matrix cracking repair and filling using active and passive modes for smart timed release of chemicals from fibers into cement matrices, Smart Mater. Struct. 3 (2) (1994), https://doi.org/10.1088/0964-1726/3/2/006.
[7] C.M. Dry, Smart multiphase composite materials that repair themselves by a release of liquids that become solids. Smart Structures and Materials, 1994, Smart Materials 2189 (1994), https://doi.org/10.1117/12.174085.
[8] G. Anglani, P. Antonaci, S.I. Carillo Gonzales, G. Paganelli, J.M. Tulliani, 3D printed capsules for self-healing concrete applications. https://doi.org/10.21012/fc10.235356, 2019.
[9] G. Anglani, T. Van Mullem, X. Zhu, J. Wang, P. Antonaci, N. De Belie, J.M. Tulliani, K. Van Tittelboom, Sealing efficiency of cement-based materials containing extruded cementitious capsules, Construct. Build. Mater. 251 (2020), https://doi.org/10.1016/j.conbuildmat.2020.119039.
[10] G. Anglani, T. Van Mullem, J.-M. Tulliani, K. Van Tittelboom, N. De Belie, P. Antonaci, Durability of self-healing cementitious systems with encapsulated polyurethane evaluated with a new prestandard test method, Mater. Struct. 55 (143) (2022), https://doi.org/10.1617/s11527-021-01818-3.
[11] S. Papaioannou, M. Amenta, V. Kilikoglou, D. Gournis, I. Karatasios, Synthesis and integration of cement-based capsules modified with sodium silicate for developing self-healing cements, Construct. Build. Mater. 316 (2022), https://doi.org/10.1016/j.conbuildmat.2021.125803.
[12] M. Araújo, S. Chatrabhuti, S. Gurdebeke, N. Alderete, K. Van Tittelboom, J. M. Raquez, V. Cnudde, S. Van Vlierberghe, N. De Belie, E. Gruyaert, Poly(methyl methacrylate) capsules as an alternative to the proof-of-concept glass capsules used in self-healing concrete, Cement Concr. Compos. 89 (2018), https://doi.org/10.1016/j.cemconcomp.2018.02.015.
[13] A. Kanellopoulos, T.S. Qureshi, A. Al-Tabbaa, Glass encapsulated minerals for self-healing in cement based composites, Construct. Build. Mater. 98 (2015), https://doi.org/10.1016/j.conbuildmat.2015.08.127.
[14] T.S. Qureshi, A. Kanellopoulos, A. Al-Tabbaa, Encapsulation of expansive powder minerals within a concentric glass capsule system for self-healing concrete, Construct. Build. Mater. 121 (2016), https://doi.org/10.1016/j.conbuildmat.2016.06.030.
[15] T. Van Mullem, G. Anglani, M. Dudek, H. Vanoutrive, G. Bumanis, C. Litina, A. Kwiecień, A. Al-Tabbaa, D. Bajare, T. Stryszewska, R. Caspeele, K. Van Tittelboom, J.M. Tulliani, E. Gruyaert, P. Antonaci, N. De Belie, Addressing the need for standardization of test methods for self-healing concrete: an inter-laboratory study on concrete with macrocapsules, Sci. Technol. Adv. Mater. 21 (1) (2020), https://doi.org/10.1080/14686996.2020.1814117.
[16] F.A. Gilabert, K. Van Tittelboom, E. Tsangouri, D. Van Hemelrijck, N. De Belie, W. Van Paepegem, Determination of strength and debonding energy of a glass-concrete interface for encapsulation-based self-healing concrete, Cement Concr. Compos. 79 (2017), https://doi.org/10.1016/j.cemconcomp.2017.01.011.
[17] B. Šavija, J. Feiteira, M. Araújo, S. Chatrabhuti, J.M. Raquez, K. Van Tittelboom, E. Gruyaert, N. De Belie, E. Schlangen, Simulation-aided design of tubular polymeric capsules for self-healing concrete, Materials 10 (1) (2017), https://doi.org/10.3390/ma10010010.
[18] C. Vlachakis, J. McAlorum, M. Perry, 3D printed cement-based repairs and strain sensors, Autom. ConStruct. 137 (2022), https://doi.org/10.1016/j.autcon.2022.104202.
[19] C. De Nardi, D. Gardner, A.D. Jefferson, Development of 3D printed networks in self-healing concrete, Materials 13 (6) (2020), https://doi.org/10.3390/ma13061328.
[20] N.A. Elkasabgy, A.A. Mahmoud, A. Maged, 3D printing: an appealing route for customized drug delivery systems, Int. J. Pharm. 588 (2020), https://doi.org/10.1016/j.ijpharm.2020.119732.
[21] V.M. Vaz, L. Kumar, 3D printing as a promising tool in personalized medicine, AAPS PharmSciTech 22 (1) (2021), https://doi.org/10.1208/s12249-020-01905-8.
[22] B. Coppola, T. Lacondemine, C. Tardivat, L. Montanaro, P. Palmero, Designing alumina-zirconia composites by DLP-based stereolithography: microstructural tailoring and mechanical performances, Ceram. Int. 47 (10) (2021), https://doi.org/10.1016/j.ceramint.2021.01.204.
[23] K. Wang, X. Gou, L. Peng, L. Du, In situ sustained-release microcapsules to improve the impermeability of cement mortars: preparation and characterization, J. Mater. Civ. Eng. 35 (6) (2023), https://doi.org/10.1061/JMCEE7.MTENG-14551.
[24] T. Lu, B. Li, D. Sun, M. Hu, J. Ma, G. Sun, Advances in controlled release of microcapsules and promising applications in self-healing of asphalt materials, J. Clean. Prod. 294 (2021), https://doi.org/10.1016/j.jclepro.2021.126270.
[25] B. Hilloulin, K. van Tittelboom, E. Gruyaert, N. de Belie, A. Loukili, Design of polymeric capsules for self-healing concrete, Cement Concr. Compos. 55 (2015) 298–307, https://doi.org/10.1016/J.CEMCONCOMP.2014.09.022.